IV International Conference on Particle-based Methods – Fundamentals and Applications
PARTICLES 2015
E. Oñate, M. Bischoff, D.R.J. Owen, P. Wriggers & T. Zohdi (Eds)

DEFORMATION OF A DROPLET IN COUETTE FLOW SUBJECT TO AN EXTERNAL ELECTRIC FIELD SIMULATED USING ISPH

NIMA TOFIGHI, MURAT OZBULUT AND MEHMET YILDIZ

Faculty of Engineering and Natural Sciences (FENS), Sabanci University,
Orhanli, Tuzla, 34956 Istanbul, Turkey
e-mails: nima@sabanciuniv.edu
ozbulut@sabanciuniv.edu
meyildiz@sabanciuniv.edu

Key words: Smoothed Particle Hydrodynamics, Droplet Deformation, Electrohydrodynamics

Abstract. Incompressible smoothed particle hydrodynamics method has been used to simulate the deformation of a two-dimensional liquid droplet suspended in Couette flow in presence of an external electric field. The results show that the elongation and orientation of the droplet is dependent on permittivity and conductivity ratios.

1 INTRODUCTION

The interaction between liquid droplets with a fluid environment is one of the most common problems arising in nature and industry, particularly in emulsification, mixing and suspensions. Simulation of the behavior of droplets in linear shear has attracted much attention where either of the droplet or the background flow may be Newtonian or non-Newtonain [1–3]. Special attention has been paid to stable rotation of droplets or their breakup. Evolution of a Newtonian droplet in non-Newtonain background fluid is studied in [1, 3] while the effects of an external electric field in a Newtonian-Newtonian case is investigated in [2].

In this study, a two-dimensional Incompressible Smoothed Particle Hydrodynamics (ISPH) scheme is used to simulate the two-phase flow of a droplet in simple shear [4]. Both fluids are modeled as leaky dielectric material [5, 6]. We have carried out numerical simulations of a Newtonian droplet in non-Newtonian background flow in a recent study [3]. Here, we extend that study to evolution of droplets in linear shear while they are exposed to an external electric field. Comparison of results with those without electric field shows that it is possible to manipulate the elongation and orientation of the droplets, as suggested by [2].

2 GOVERNING EQUATIONS

Equations governing an incompressible flow may be written as

$$\nabla \cdot \mathbf{u} = 0, \tag{1}$$

$$\rho \frac{\mathrm{D}\mathbf{u}}{\mathrm{D}t} = -\nabla p + \frac{1}{\mathrm{Re}} \nabla \cdot \boldsymbol{\tau} + \frac{1}{\mathrm{We}} \mathbf{f}_{(s)} + \frac{1}{\mathrm{Ei}} \mathbf{f}_{(e)}, \tag{2}$$

where $\mathbf{u}$ is the velocity vector, p is pressure, ρ is density, t is time and $\mathrm{D}/\mathrm{D}t = \partial/\partial t + \mathbf{u} \cdot \boldsymbol{\nabla}$ represents the material time derivative. Here, $\boldsymbol{\tau}$ is the viscous stress tensor,

$$\boldsymbol{\tau} = \mu \left[\boldsymbol{\nabla}\mathbf{u} + (\boldsymbol{\nabla}\mathbf{u})^{\dagger} \right], \tag{3}$$

where μ denotes viscosity and superscript $\square^{\dagger}$ represents the transpose operation. Local surface tension force is expressed as an equivalent volumetric force according to the CSF method [7],

$$\mathbf{f}_{(s)} = \gamma \kappa \hat{\mathbf{n}} \delta. \tag{4}$$

Here, surface tension coefficient, γ, is taken to be constant while κ represents interface curvature, $-\nabla \cdot \hat{\mathbf{n}}$, where $\hat{\mathbf{n}}$ is unit surface normal vector. $\mathbf{f}_{(e)}$ is the electric force vector defined as [5]

$$\mathbf{f}_{(e)} = -\frac{1}{2} \mathbf{E} \cdot \mathbf{E} \boldsymbol{\nabla} \varepsilon + q^{v} \mathbf{E}. \tag{5}$$

In the above equation, ε denotes electric permittivity, q^{v} is the volume charge density near the interface while $\mathbf{E}$ is the electric field vector. Assuming small dynamic currents and neglecting magnetic induction effects, the electric field is irrotational [8] and may be represented by gradient of an electric potential ϕ, $\mathbf{E} = -\boldsymbol{\nabla}\phi$. Further assumption of fast electric relaxation time compared to viscous relaxation time leads to the following relations for electric potential and charge density

$$\boldsymbol{\nabla} \cdot (\sigma \boldsymbol{\nabla} \phi) = 0, \tag{6}$$

$$q^{v} = \boldsymbol{\nabla} \cdot (\varepsilon \boldsymbol{\nabla} \phi), \tag{7}$$

where σ is the electrical conductivity.

Dimensionless values are formed using the following scales

$$\begin{aligned} &\mathbf{x} = \mathbf{x}^{*}/H, \quad \rho = \rho^{*}/\rho_f, \quad \mu = \mu^{*}/\mu_f \quad \mathbf{u} = \mathbf{u}^{*}/U_w, \quad t = t^{*}U_w/H, \\ &\mathbf{E} = \mathbf{E}^{*}/E_{\infty}, \quad \phi = \phi^{*}/E_{\infty}H, \quad p = p^{*}/\rho_f U_w^2, \\ &\mathcal{R} = \rho_d/\rho_f, \quad \mathcal{M} = \mu_d/\mu_f, \quad \mathcal{P} = \varepsilon_d/\varepsilon_f, \quad \mathcal{C} = \sigma_d/\sigma_f, \end{aligned} \tag{8}$$

leading to Reynolds, Weber and Electroinertial numbers defined as

$$\mathrm{Re} = \frac{\rho_f U_w H}{\mu_f}, \quad \mathrm{We} = \frac{\rho U_w^2 H}{\gamma}, \quad \mathrm{Ei} = \frac{\rho_f U_w^2}{\varepsilon_f E_{\infty}^2}. \tag{9}$$

Here E_∞ is the undisturbed electric field intensity, H is the distance between electrodes, U_w is the wall velocity (figure 1-a). An asterisk marks dimensional variables whereas subscripts $\square_d$ and $\square_f$ denote droplet and background fluid phases, respectively.

To distinguish between different phases, a color function $\hat{c}$ is defined such that it assumes a value of zero for one phase and unity for the other. The color function is then smoothed out across the phase boundaries as

$$c_{\mathrm{i}} = \sum_{\mathrm{j}=1}^{J_n} \frac{\hat{c}_{\mathrm{j}} W_{\mathrm{ij}}}{\psi_{\mathrm{i}}}, \tag{10}$$

to ensure smooth transition between the properties of each phase when used for their interpolation. Here, $\psi_{\mathrm{i}} = \sum_{\mathrm{j}=1}^{J_n} W_{\mathrm{ij}}$, is the number density of SPH particle i, calculated as the sum of interpolation kernel of neighboring particles i and j over all neighbors of particle i, J_n. Interpolation kernel, $W(r_{\mathrm{ij}}, h)$, is a function of the magnitude of distance vector, $\mathbf{r}_{\mathrm{ij}} = \mathbf{r}_{\mathrm{i}} - \mathbf{r}_{\mathrm{j}}$, between particle of interest i and its neighboring particles j and h, the smoothing length [9, 10]. Interpolation of phase properties is carried out using Weighted Harmonic Mean (WHM),

$$\frac{1}{\chi_{\mathrm{i}}} = \frac{c_{\mathrm{i}}}{\chi_d} + \frac{1 - c_{\mathrm{i}}}{\chi_f}, \tag{11}$$

where χ may denote density, viscosity, permittivity or conductivity [11]. The smoothed color function is also utilized to evaluate $\delta \simeq |\nabla c|$, $\kappa = -\nabla \cdot \hat{\mathbf{n}}$ and $\hat{\mathbf{n}} = \nabla c / |\nabla c|$ in (4). In this formulation, a constraint has to be enforced to avoid possible erroneous normals [12]. In this study, only gradient values exceeding a certain threshold, $|\nabla c_{\mathbf{i}}| \simeq \beta / h$, are used in surface tension force calculations. A β value of 0.08 has been found to provide accurate results without removing too much detail [4].

A predictor-corrector scheme is employed to advance the governing equations of flow in time using a first-order Euler approach with variable timestep according to Courant-Friedrichs-Lewy condition, $\Delta t = C_{CFL} h / u_{max}$, where u_{max} is the largest particle velocity magnitude and C_{CFL} is taken to be equal to 0.25. In predictor step all the variables are advanced to their intermediate form using following relations,

$$\mathbf{r}_{\mathrm{i}}^{*} = \mathbf{r}_{\mathrm{i}}^{(n)} + \mathbf{u}_{\mathrm{i}}^{(n)} \Delta t + \boldsymbol{\delta}\mathbf{r}_{\mathrm{i}}^{(n)}, \tag{12}$$

$$\mathbf{u}_{\mathrm{i}}^{*} = \mathbf{u}_{\mathrm{i}}^{(n)} + \frac{1}{\rho_{\mathrm{i}}^{(n)}} \left(\frac{1}{\mathrm{Re}} \nabla \cdot \boldsymbol{\tau}_{\mathrm{i}} + \frac{1}{\mathrm{We}} \mathbf{f}_{(s)\mathrm{i}} + \frac{1}{\mathrm{Ei}} \mathbf{f}_{(e)\mathrm{i}} \right)^{(n)} \Delta t, \tag{13}$$

$$\psi_{\mathrm{i}}^{*} = \psi_{\mathrm{i}}^{(n)} - \Delta t \psi_{\mathrm{i}}^{(n)} \left(\nabla \cdot \mathbf{u}_{\mathrm{i}}^{*} \right), \tag{14}$$

where starred variables represent intermediate values and superscript (n) denotes values at the nth time step. Artificial particle displacement vector in (12), $\boldsymbol{\delta}\mathbf{r}_{\mathrm{i}}$, is defined as stated in [3] where a constant value of 0.06 is used.

Using intermediate values, pressure at the next time step is found by solving the Poisson equation which is then followed by corrections in position and velocity of the particles, completing the temporal transition.

$$\nabla \cdot \left(\frac{1}{\rho_{\mathrm{i}}^{*}} \nabla p_{\mathrm{i}}^{(n+1)} \right) = \frac{\nabla \cdot \mathbf{u}_{\mathrm{i}}^{*}}{\Delta t}, \tag{15}$$

$$\mathbf{u}_{\mathrm{i}}^{(n+1)} = \mathbf{u}_{\mathrm{i}}^{*} - \frac{1}{\rho_{\mathrm{i}}^{*}} \nabla p_{\mathrm{i}}^{(n+1)} \Delta t, \tag{16}$$

$$\mathbf{r}_{\mathrm{i}}^{(n+1)} = \mathbf{r}_{\mathrm{i}}^{(n)} + \frac{1}{2} \left(\mathbf{u}_{\mathrm{i}}^{(n)} + \mathbf{u}_{\mathrm{i}}^{(n+1)} \right) \Delta t + \boldsymbol{\delta} \mathbf{r}_{\mathrm{i}}^{(n)}. \tag{17}$$

Boundary conditions are enforced through MBT method described in [13] while first derivative and Laplace operator are approximated through following expressions

$$\frac{\partial f_{\mathrm{i}}^{m}}{\partial x_{\mathrm{i}}^{k}} a_{\mathrm{i}}^{kl} = \sum_{\mathrm{j}} \frac{1}{\psi_{\mathrm{j}}} \left(f_{\mathrm{j}}^{m} - f_{\mathrm{i}}^{m} \right) \frac{\partial W_{\mathrm{ij}}}{\partial x_{\mathrm{i}}^{l}}, \tag{18}$$

$$\frac{\partial^2 f_{\mathrm{i}}^{m}}{\partial x_{\mathrm{i}}^{k} \partial x_{\mathrm{i}}^{k}} a_{\mathrm{i}}^{ml} = 8 \sum_{\mathrm{j}} \frac{1}{\psi_{\mathrm{j}}} \left(f_{\mathrm{i}}^{m} - f_{\mathrm{j}}^{m} \right) \frac{r_{\mathrm{ij}}^{m}}{r_{\mathrm{ij}}^{2}} \frac{\partial W_{\mathrm{ij}}}{\partial x_{\mathrm{i}}^{l}}. \tag{19}$$

Here, $a_{\mathrm{i}}^{kl} = \sum_{\mathrm{j}} \frac{r_{\mathrm{ij}}^{k}}{\psi_{\mathrm{j}}} \frac{\partial W_{\mathrm{ij}}}{\partial x_{\mathrm{i}}^{l}}$ is a corrective second rank tensor that eliminates particle inconsistencies. Left hand side of (15) is discretized as

$$\frac{\partial^2 f_{\mathrm{i}}^{m}}{\partial x_{\mathrm{i}}^{k} \partial x_{\mathrm{i}}^{k}} \left(2 + a_{\mathrm{i}}^{kk} \right) = 8 \sum_{\mathrm{j}} \frac{1}{\psi_{\mathrm{j}}} \left(f_{\mathrm{i}}^{m} - f_{\mathrm{j}}^{m} \right) \frac{r_{\mathrm{ij}}^{k}}{r_{\mathrm{ij}}^{2}} \frac{\partial W_{\mathrm{ij}}}{\partial x_{\mathrm{i}}^{k}}. \tag{20}$$

3 RESULTS

In this study, deformation of a neutrally buoyant droplet suspended in plane Couette flow is simulated. The droplet is expected to elongate in the direction of flow, possibly reaching an equilibrium dictated by the balance between the forces acting on the interface [3]. A schematic of this case is provided in figure 1-a. Computational domain consists of an 8×32 rectangle discretized by 39973 particles initially arranged in a Cartesian grid for background fluid and concentric circles for the droplet [14]. A close-up view of the particle arrangement in the vicinity of the droplet is provided in figure 1-b. Initial droplet radius is half of the distance between moving walls, $H/2$, while the droplet is placed at the center of the channel. Top and bottom walls abide by the no-slip condition and are moving in opposite directions at a velocity of $U_w/2$ while applying a potential difference of $\Delta\phi = E_\infty H$. Periodic boundary condition is imposed in streamwise direction. Particles inside the droplet are at rest while background fluid particles are initialized with undisturbed Couette flow velocity. Reynolds, Weber and Electroinertial numbers are set to 1, 0.2 and 50, respectively. The background and droplet fluids have identical density

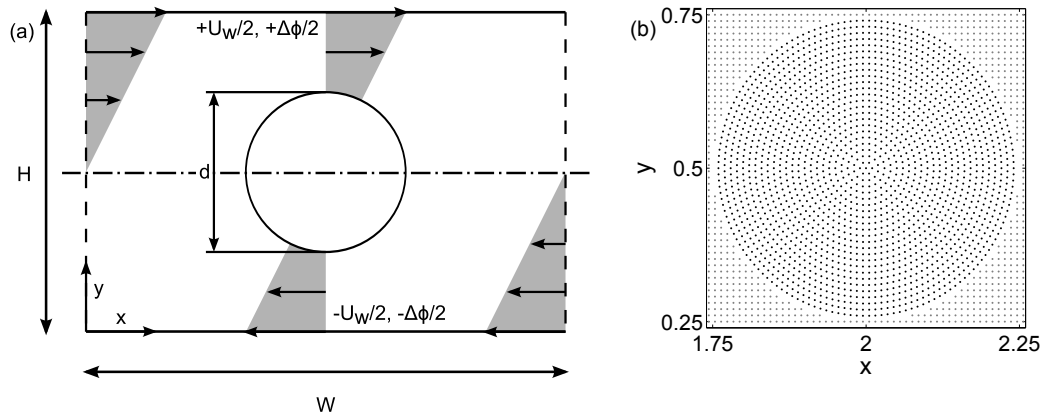

Figure 1: (a) Schematic of the test case. (b) Closeup view of initial particle distribution in the vicinity of the droplet. Black points denote droplet particles whereas gray points are background fluid particles.

and viscosity while permittivity and conductivity ratios are varied according to table 1. Equal permittivity and conductivity ratios are not considered here.

Figure 2 provides droplet deformation factor defined as

$$D_f = \frac{L_{max} - L_{min}}{L_{max} + L_{min}}, \tag{21}$$

where L_{max} and L_{min} denote major and minor axis of an approximated ellipsoid [15]. Denoting the test cases in pairs of permittivity and conductivity ratios as $(\mathcal{P}, \mathcal{C})$, cases $(5.0, 0.2)$ and $(5.0, 0.5)$ do not reach a steady profile during the simulation time. Observing the deformation rate of case $(5.0, 0.2)$, we predict that the droplet will eventually breakup, given sufficient simulation time. Averaged values of D_f are provided in table 1 for better comparison. At constant $\mathcal{P}$, increasing $\mathcal{C}$ results in larger deformation factors for $\mathcal{P} < 1$ while this trend is reversed for $\mathcal{P} > 1$. Similarly, at constant $\mathcal{C}$, a larger $\mathcal{P}$ results in larger D_f for $\mathcal{C} < 1$ while increasing $\mathcal{P}$ for $\mathcal{C} > 1$ reduces the deformation factor.

Figure 3 provides a better representation of the interface profile at the end of the simulations. Smoothed color function is used to define the droplet interface by plotting its contour at 0.5 level. The droplets are more slender where deformation factor is larger (refer to table 1). It is notable that the angle between major axis of the elliptic droplet and streamwise direction becomes smaller with increasing conductivity ratio. The shape of case $(5.0, 0.2)$ is immediately distinguishable due to its large deformation. As $\mathbf{f}_{(e)}$ increases with $\mathcal{P}$, the extreme elongation happens as a result of suppression of surface tension forces by electrical forces. It is also notable that the droplet has lost its elliptic shape at this simulation time.

Figure 4 provides snapshots of interface in red, streamlines in blue and electric field lines in black for the case without electric field, case with largest elongation $(5.0, 0.2)$ and two other cases. The last two cases, $(0.2, 2.0)$ and $(2.0, 0.2)$, are chosen based on their

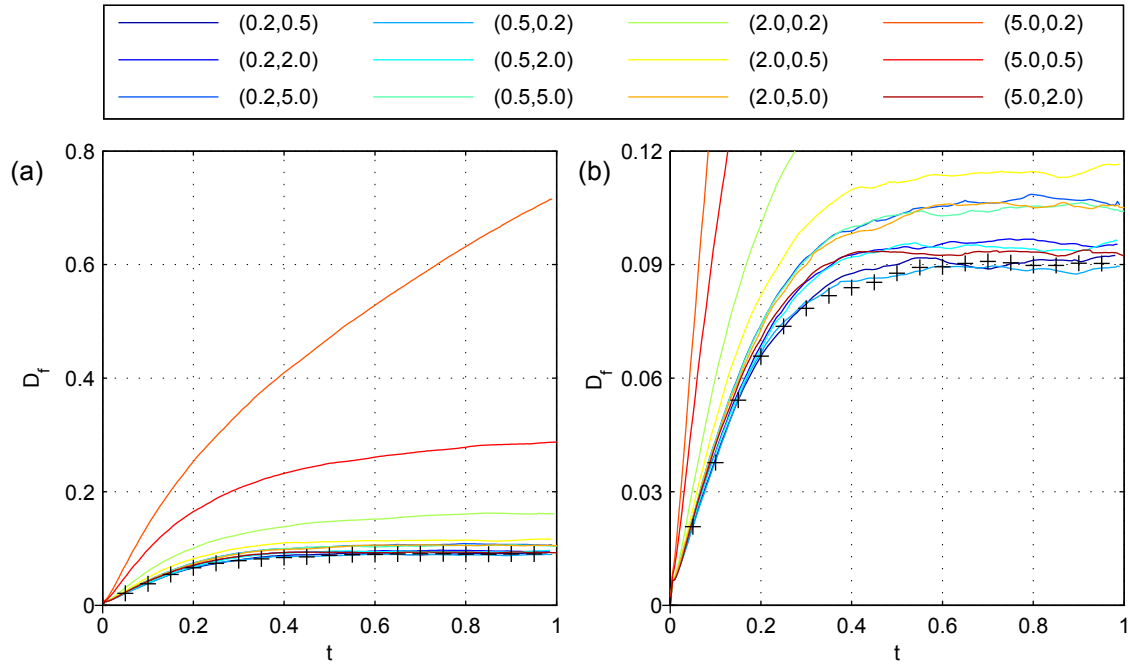

Figure 2: Comparison of the deformation factor for all cases (a) and a close up view of the cases with steady shape (b). Black plus signs denote the case without electric field.

Table 1: Deformation factor for different permittivity and conductivity ratios. Cases with bold numbers did not reach a steady profile during the simulation. Deformation factor without electric field is $D_f = 0.09$.

$\mathcal{P}$		0.2	0.5	2	5
$\mathcal{C}$	0.2	-	0.089	0.162	**0.675**
	0.5	0.091	-	0.115	**0.284**
	2	0.096	0.094	-	0.093
	5	0.107	0.105	0.105	-

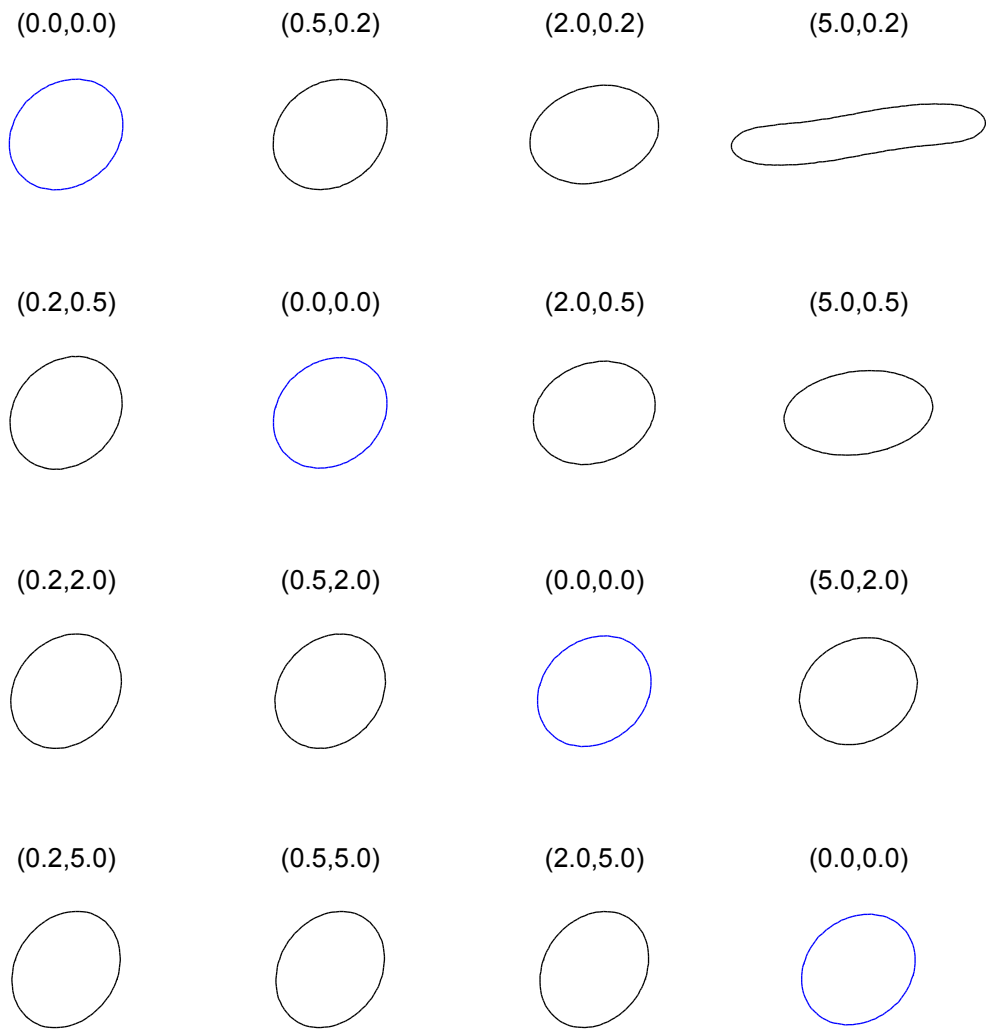

Figure 3: Interface profiles of droplet at the end of the simulation. Permittivity and conductivity pairs $(\mathcal{P}, \mathcal{C})$ are shown above each case. The case with no electric field, shown in blue, is repeated in each row marked as $(0.0, 0.0)$.

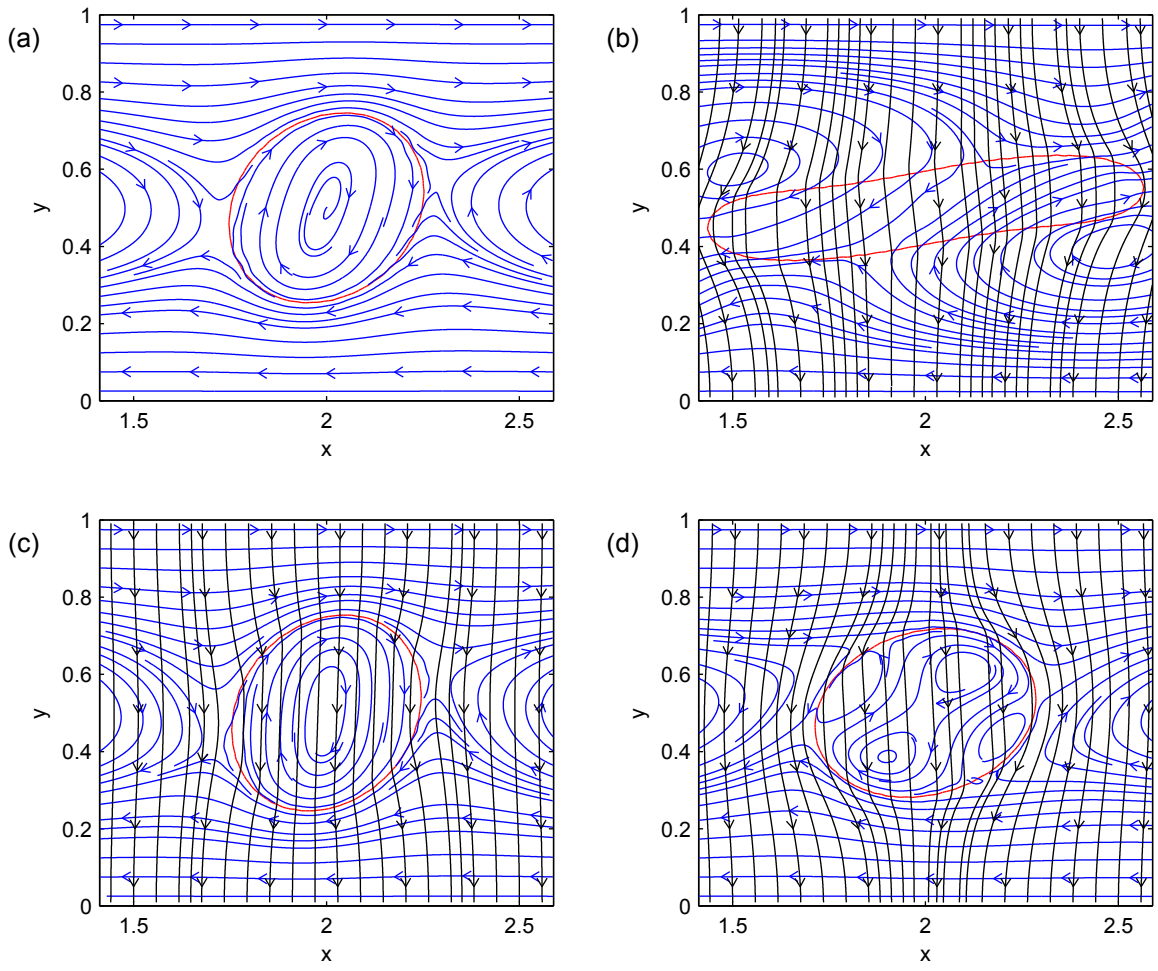

Figure 4: Snapshots of droplet interface in red, streamlines in blue and electric field lines in black at the end of simulation; (a) without electric field; (b) $(5.0, 0.2)$; (c) $(0.2, 2.0)$; (d) $(2.0, 0.2)$.

final orientation when compared to the case without electric field. Case $(0.2, 2.0)$ is more aligned to normal direction wheres $(2.0, 0.2)$ is more aligned to streamwise direction. Case without electric field shows a circulation region inside droplet while two types of streamlines in background fluid are observed. The first type traverses the whole domain while the second type approaches the droplet and then reverses its direction. Case $(5.0, 0.2)$ shows no circulation inside the droplet while two large vortices are observed near trailing edges of the droplet. These vortices encompass both droplet and background fluid and rotate in the direction of imposed shear. Since the droplet is less conductive than the surrounding fluid in this case, the electric field lines diverge from the surface of the droplet. The streamlines in case $(0.2, 2.0)$ resemble those of the case without electric field in general. Electric field lines converge toward the droplet as it is more conductive than surrounding fluid in this case. The streamlines in case $(2.0, 0.2)$ start to show a different pattern than that of the case with no electric field. A pattern similar to the case without shear, that is four vortical structure rotating alternatively in clockwise and counterclockwise rotations [8], is observed here. The vortices rotating in the direction of background flow's vorticity are paired, separating the voritces countering the imposed shear. With a conductivity ratio of $\mathcal{C} = 0.2$, the droplet is less conductive than surrounding fluid and the electric field lines diverge from the droplet surface.

4 CONCLUSION

In this paper, we use ISPH to simulate the deformation of a neutrally buoyant droplet in planar Couette flow under external electric field. The deformation factor is compared for different permittivity and conductivity ratios. It is seen that it is possible to overcome the surface tension forces at suitable permittivity and conductivity ratios, resulting in droplet elongations that are likely to end in breakup. The effects of permittivity and conductivity ratios on streamline patterns are also studied. It is seen that the circulation patterns may change for cases with a preference for aligning with the streamwise direction, resulting in patterns resembling those observed in the absence of imposed shear.

5 ACKNOWLEDGMENTS

The authors gratefully acknowledge financial support provided by the Scientific and Technological Research Council of Turkey (TUBITAK) for project number 112M721.

REFERENCES

[1] Chinyoka, T., Renardy, Y., Renardy, A. and Khismatullin, D. Two-dimensional study of drop deformation under simple shear for Oldroyd-B liquids. *J. Non-Newton. Fluid Mech.* (2005) **130**:45-56.

[2] Maehlmann, S. and Papageorgiou, D.T. Numerical study of electric field effects on the deformation of two-dimensional liquid drops in simple shear flow at arbitrary Reynolds number. *J. Fluid Mech.* (2009) **626**:367-393.

[3] Zainali, A., Tofighi, N., Shadloo, M.S. and Yildiz, M. Numerical investigation of Newtonian and non-Newtonian multiphase flows using ISPH method. *Comput. Meth. Appl. Mech. Eng.* (2013) **254**:99–113.

[4] Tofighi, N. and Yildiz, M. Numerical simulation of single droplet dynamics in three-phase flows using ISPH. *Comput. Math. Appl.* (2013) **66**:525-536.

[5] Saville, D. Electrohydrodynamics: The Taylor-Melcher leaky dielectric model. *Annu. Rev. Fluid Mech.* (1997) **29**:27-64.

[6] Shadloo, M., Rahmat, A. and Yildiz, M. A smoothed particle hydrodynamics study on the electrohydrodynamic deformation of a droplet suspended in a neutrally buoyant Newtonian fluid. *Comput. Mech.* (2013) 1-15.

[7] Brackbill, J., Kothe, D. and Zemach, C. A continuum method for modeling surface-tension. *J. Comput. Phys.* (1992) **100**:335-354.

[8] Hua, J., Lim, L. and Wang, C. Numerical simulation of deformation/motion of a drop suspended in viscous liquids under influence of steady electric fields. *Phys. Fluids* (2008) **20**:113302.

[9] Monaghan, J.J. and Lattanzio, J.C. A refined particle method for astrophysical problems. *Astron. Astrophys.* (1985) **149**:135–143.

[10] Monaghan, J.J. and Kocharyan, A. SPH simulation of multiphase flow. *Comput. Phys. Commun.* (1995) **87**:225–235.

[11] Tomar, G., Gerlach, D., Biswas, G., Alleborn, N., Sharma, A., Durst, F., Welch, S.W.J. and Delgado, A. Two-phase electrohydrodynamic simulations using a volume-of-fluid approach. *J. Comput. Phys.* (2007) **227**:1267-1285.

[12] Morris, J.P. Simulating surface tension with smoothed particle hydrodynamics. *Int. J. Numer. Methods Fluids* (2000) **33**:333-353.

[13] Yildiz, M., Rook, R.A. and Suleman, A. SPH with the multiple boundary tangent method. *Int. J. Numer. Methods Eng.* (2009) **77**:1416–1438.

[14] Tofighi, N., Ozbulut, M., Rahmat, A., Feng, J.J. and Yildiz, M. An incompressible smoothed particle hydrodynamics method for the motion of rigid bodies in fluids. *J. Comp. Phys.* (2015) **297**:207 - 220.

[15] Taylor, G. Studies in electrohydrodynamics .I. Circulation produced in a drop by an electric field. *Proc. R. Soc. Lon. Ser. A* (1966) **291**:159-166.